Energy & Environmental Science

COMMUNICATION

Cite this: *Energy Environ. Sci.*, 2015, **8**, 2941

Received 27th July 2015,
Accepted 9th September 2015

DOI: 10.1039/c5ee02315g

www.rsc.org/ees

A zinc–iron redox-flow battery under $100 per kW h of system capital cost†

Ke Gong,[a] Xiaoya Ma,[a] Kameron M. Conforti,[b] Kevin J. Kuttler,[a] Jonathan B. Grunewald,[a] Kelsey L. Yeager,[a] Martin Z. Bazant,[bc] Shuang Gu*[a] and Yushan Yan*[a]

Redox flow batteries (RFBs) are one of the most promising scalable electricity-storage systems to address the intermittency issues of renewable energy sources such as wind and solar. The prerequisite for RFBs to be economically viable and widely employed is their low cost. Here we present a new zinc–iron (Zn–Fe) RFB based on double-membrane triple-electrolyte design that is estimated to have under $100 per kW h system capital cost. Such a low cost is achieved by a combination of inexpensive redox materials (*i.e.*, zinc and iron) and high cell performance (*e.g.*, 676 mW cm^{-2} power density). Engineering of the cell structure is found to be critical to enable the high power density. Our cost model shows that a Zn–Fe RFB demonstrates the lowest cost among some notable RFBs and could reach the 2023 cost target set by the U.S. Department of Energy ($150 per kW h).

Broader context

The widespread deployment of renewable energies such as wind and solar calls for energy-storage systems to smooth out their intermittent electricity generation. Redox-flow batteries (RFBs) are scalable energy-storage devices with great design flexibility due to their decoupled energy and power functions. The most important prerequisite for RFBs to be economically viable is low capital cost. In this work, we present a zinc–iron (Zn–Fe) RFB that uses inexpensive redox materials yet offers high cell performance, and thus achieves a very low system capital cost under $100 per kW h.

The widespread deployment of renewable energies such as wind and solar calls for energy-storage systems to smooth out their intermittent electricity generation. Various technologies have been introduced, including physical methods such as pumped hydro and compressed air, and electrochemical methods such as regenerative fuel cells and rechargeable batteries.[1–7] Redox flow batteries (RFBs) are one of the most promising systems due to their excellent scalability. Freeing the redox pairs from the solid electrodes into flowing electrolytes allows independent engineering for energy (through electrolytes) and power (through electrodes), leading to flexibility in system design and deployment.[8–12] One of the prerequisites for RFBs to be widely employed in energy storage is their low capital cost. To make electricity-storage systems economically viable, the US Department of Energy has set a system capital cost target of $150 per kW h by 2023,[13] and an even lower target of $100 per kW h is needed to match the existing grid-level storage technologies of pumped hydro and compressed air. However, these targets have not been met so far due to the high cost of redox pairs and/or the low power density of cells. For example, the most developed all-vanadium (denoted as all-V) RFBs currently have a system capital cost around ~$300–$800 per kW h.[14] Here we design a new RFB that uses low-cost redox pairs (*i.e.*, zinc and iron, denoted as a Zn–Fe RFB) and demonstrates high power density (*e.g.*, 676 mW cm^{-2}); the Zn–Fe RFB therefore offers a potential system capital cost of less than $100 per kW h.

The RFB system cost has two major contributions: electrolyte cost and stack cost:

$$C_{sys} \approx C_e + C_s = U_e/V_{eff} + U_s/(t{\cdot}I{\cdot}V_{eff}) \quad (1)$$

where, C_{sys}, C_e and C_s are the system, electrolyte and stack cost ($ per kW h), respectively; U_e is the unit cost of the electrolyte including redox elements and supporting salts/acids/bases ($ per A h); U_s is the unit cost of the stack including electrodes, membranes and bipolar plates ($ per m^2); V_{eff} is the effective discharge cell voltage (V); t is the designed discharge duration (h); and I is the current density (A m^{-2}).

From eqn (1), a low system cost can be achieved by minimizing U_e and/or U_s, or maximizing V_{eff}. Low U_e and U_s can be obtained by using low cost redox pairs and stack materials, while high V_{eff} requires high reversible cell voltage, and small overpotential and internal resistance, as shown in eqn (2).

$$V_{eff} = V_{rev} - \eta - I{\cdot}R \quad (2)$$

[a] *Department of Chemical and Biomolecular Engineering, University of Delaware, Newark, Delaware 19716, USA. E-mail: shuang.gu@wichita.edu, yanys@udel.edu*
[b] *Department of Chemical Engineering, Massachusetts Institute of Technology, Cambridge, Massachusetts 02139, USA*
[c] *Department of Mathematics, Massachusetts Institute of Technology, Cambridge, Massachusetts 02139, USA*

† Electronic supplementary information (ESI) available. See DOI: 10.1039/c5ee02315g

where, V_{rev} is the reversible voltage, η is the total activation overpotential at both electrodes (V), I is the current density and R is the area-specific internal cell resistance (Ω cm^2).

Current RFBs cannot satisfy simultaneously low U_e and high V_{eff} at high current densities. As a reference, the challenges facing two notable RFBs are described here. All-V RFBs recently achieved a dramatic improvement in their V_{eff} at high current density by reduction of internal resistance, but their U_e is too high.[15] The vanadium material alone would cost $64 per kW h (Table S1, ESI†). On the other hand, Cr–Fe RFBs have low U_e, but their V_{eff} is low due to the intrinsically low reversible cell voltage and sluggish kinetics of the Cr redox pair.[16] It is therefore imperative to find two redox pairs that have low elemental cost, fast redox kinetics, and high reversible voltage.

Zn and Fe are two elements with the potential to satisfy these low cost requirements. Specifically, the use of Zn in a basic environment and Fe in an acidic environment has been seen in many RFBs due to their low elemental cost, facile redox kinetics, and desirable standard potential ($\phi_{Zn(II)/Zn} = -1.22$ V *vs.* SHE in base, pH = 14; and $\phi_{Fe(III)/Fe(II)} = 0.77$ V *vs.* SHE in acid, pH = 0).[17,18] In addition, the long-standing concern of Zn dendrite formation is precluded by the flowing electrolyte in RFBs.[19] Each of the two redox pairs has been separately used in the construction of many promising RFBs;[17,18,20] however, the combination of the two redox pairs in one cell cannot be realized by the conventional single-membrane cell configuration. In this work, the Zn–Fe RFB is fabricated using a double-membrane design that enables the use of redox pairs of different ion charges and supporting electrolytes of different pHs.[21] The working principles of the Zn–Fe RFB based on the basic Zn redox pair and the acidic Fe redox pair are illustrated in Fig. 1, and the negative and positive electrode reactions are shown in eqn (3) and (4), respectively.

$$\text{Negative electrode: } Zn + 4OH^- \leftrightarrow Zn(OH)_4^{2-} + 2e^- \quad (3)$$

$$\text{Positive electrode: } 2Fe^{3+} + 2e^- \leftrightarrow 2Fe^{2+} \quad (4)$$

The combination of the Zn redox pair in base and the Fe redox pair in acid has the potential to achieve very low system capital cost: (1) both Zn and Fe are inexpensive elements, *i.e.*, ¢0.13 per A h (half-cell) for Fe and ¢0.20 per A h (half-cell) for Zn (see the ESI† for calculation). Overall, a Zn–Fe RFB requires an electrolyte cost (U_e) of only ¢0.73 per A h (full-cell), which is one order of magnitude smaller than that of all-V RFBs (¢8.10 per A h, full-cell). (2) The combination of the $Zn(OH)_4^{2-}$/Zn redox pair in base and the Fe^{3+}/Fe^{2+} redox pair in acid provides a high standard cell voltage of 1.99 V and also offers a wide electrochemical window of 2.06 V for water splitting (−0.83 V of hydrogen evolution at pH = 14 and 1.23 V of oxygen evolution at pH = 0). (3) Both $Zn(OH)_4^{2-}$/Zn and Fe^{3+}/Fe^{2+} redox pairs have facile kinetics, with the standard rate constant (k^0) of 2.5×10^{-4} cm s^{-1} for the former and 1.2×10^{-4} cm s^{-1} for the latter.[22] The magnitudes of these standard rate constants require very small electrode overpotential even at high current density. For example, the charge/discharge electrode overpotential is less than 10 mV and 40 mV for the Fe^{3+}/Fe^{2+} redox pair (carbon felt electrode) and the $Zn(OH)_4^{2-}$/Zn redox pair (copper mesh electrode), respectively, at a current density of 200 mA cm^{-2} (Fig. S1, ESI†). These small overpotentials observed in this work are consistent with data reported in the literature.[19,20]

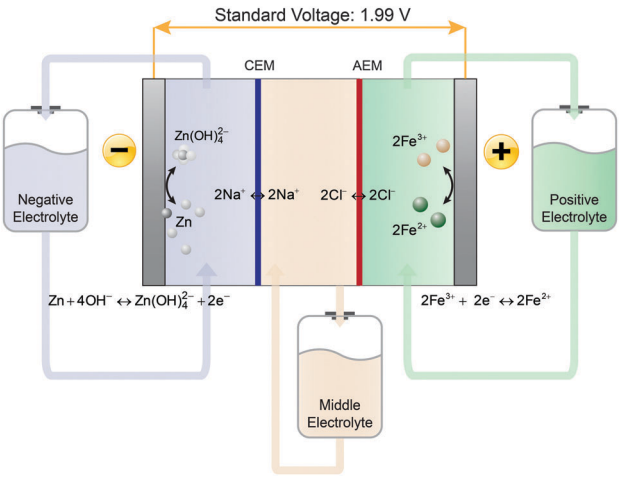

Fig. 1 Schematic of the Zn–Fe RFB. The negative electrolyte is comprised of $Zn(OH)_4^{2-}$/Zn as a negative redox pair and a NaOH solution; the middle electrolyte is a NaCl solution; the positive electrolyte is comprised of Fe^{3+}/Fe^{2+} as the positive redox pair and an HCl solution. A cation-exchange membrane (CEM) separates the negative electrolyte and the middle electrolyte while an anion-exchange membrane (AEM) separates the middle electrolyte and the positive electrolyte. The working principles are as follows. When the cell is being charged, $Zn(OH)_4^{2-}$ anions are reduced to form Zn metal deposits in the negative electrolyte, and Na^+ cations move from the middle electrolyte, passing through the CEM, to the negative electrolyte. At the same time, Fe^{2+} cations are oxidized to form Fe^{3+} cations, and Cl^- anions move from the middle electrolyte, passing through the AEM, to the positive electrolyte. As a result, the NaCl concentration in the middle electrolyte decreases in the charging process. The discharging process is the reverse of the charging process.

A sufficiently low cell resistance is then the remaining barrier to achieving the low cost. Unlike traditional single-membrane RFBs, the double-membrane design used by the Zn–Fe RFB requires an additional membrane and electrolyte, which adds challenges for managing the cell resistance. The study shows that the total cell resistance consists of two components: ohmic resistance (R_o) mostly from the two membranes and three electrolytes; and concentration-polarization resistance (R_{cp}) caused by insufficient ion diffusion in the middle electrolyte.[23] Specifically, the concentration-polarization resistance originates from the accumulation or depletion of Na^+ and Cl^- ions in the vicinity of either membrane when a current flows through the cell (Fig. S2a, ESI†). Compared with OH^- anions (in negative electrolyte) and H^+ cations (in positive electrolyte), the Na^+ cations and Cl^- anions have much smaller ion diffusion coefficients, and as such the middle electrolyte, to a great extent, controls R_{cp}.

R_o can be managed by optimizing the electrolyte concentration and reducing the thickness of the middle electrolyte (Fig. S3a and b, ESI†). With an optimal electrolyte concentration of 2.5 mol L^{-1} and a small electrolyte thickness of 0.5 mm, an R_o as low as 2.3 Ω cm^2 was obtained, which is sufficiently low for the Zn–Fe RFB, considering its close-to-2 V

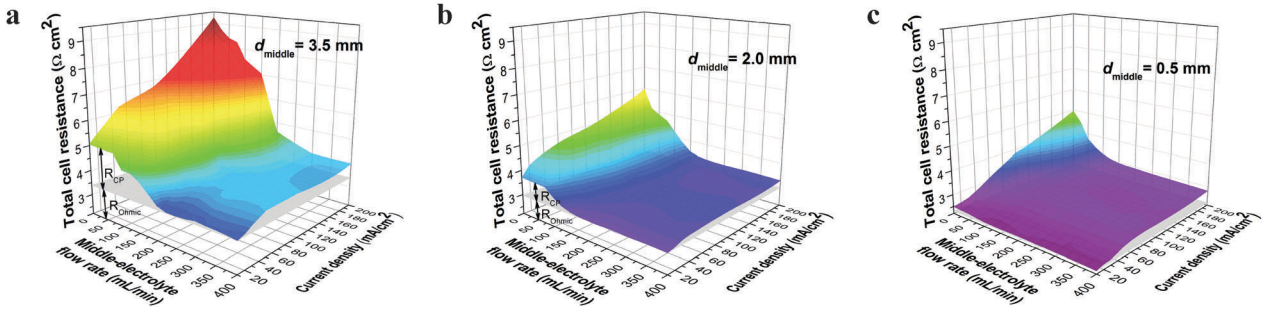

Fig. 2 The impact of the middle-electrolyte flow rate and current density on total cell resistance at different middle-electrolyte thicknesses (d_{middle}). (a) d_{middle} = 3.5 mm. (b) d_{middle} = 2.0 mm. (c) d_{middle} = 0.5 mm.

standard voltage. R_{cp}, on the other hand, depends on various structural and operational parameters[24] (Fig. S2b, ESI†). R_{cp} can be quantitatively measured by subtracting the constant R_o from total cell resistance obtained at different flow rates and/or different current densities.

Fig. 2 shows the impact of flow rate and current density on R_{cp} with different thicknesses of the middle electrolyte (0.5, 2. 0, and 3.5 mm). We found that the operational and structural parameters can be correlated to a dimensionless number X characterizing R_{cp}: $X = (Q{\cdot}d^{-1}{\cdot}w^{-1})/(I{\cdot}F^{-1}{\cdot}C^{-1})$, where, Q is the flow rate; d and w are thickness and width of the middle electrolyte, respectively; I is current density; F is the Faraday's constant; C is the salt concentration of the middle electrolyte. The quantity X represents the ratio of vertical velocity of convection (direction of electrolyte flow) to horizontal velocity of ion diffusion (direction of current flow). From regression analysis, increasing X can effectively depress R_{cp} to a negligible level (Fig. S4a, ESI†). This relationship illustrates the general resistance behavior with respect to cell structural and operational parameters. The theoretically calculated R_{cp} also has a similar trend with respect to the dimensionless number X (Fig. S4b and c, ESI†), as compared with measured R_{cp}. Both results show that R_{cp} can be limited to around 0.1 Ω cm² if X is larger than 10^5, suggesting that the manipulation of cell structural and operational parameters is effective to minimize R_{cp}.

With an engineered middle electrolyte, the Zn–Fe RFB achieves high performance (Fig. 3). A peak power density of 676 mW cm^{-2} was delivered during discharge at a current density of 660 mA cm^{-2} at 70% of state of charge (Fig. 3a, state of charge, SOC, is calculated as a percentage *via* dividing available capacity for discharge by total capacity of the battery). This peak power density is the highest among all RFBs based on zinc (~200 mW cm^{-2} for the Zn–Br RFB to our best estimation[25]) or iron (257 mW cm^{-2} for the H–Fe RFB[20]) and among the highest among advanced RFBs including quinone-Br RFBs (600 mW cm^{-2}),[26] all-V RFBs (1300 mW cm^{-2}),[27] and H–Br RFBs (1450 mW cm^{-2}).[28] In addition, even at I = 600 mA cm^{-2}, V_{eff} remains at 1.1 V, which is comparable to V_{rev} of some of the most advanced RFBs. The charge polarization also demonstrated high power density, comparable to discharge power density. Zn–Fe RFBs also showed a very high coulombic efficiency of 99.9% regardless of current density (Fig. 3b), indicating excellent

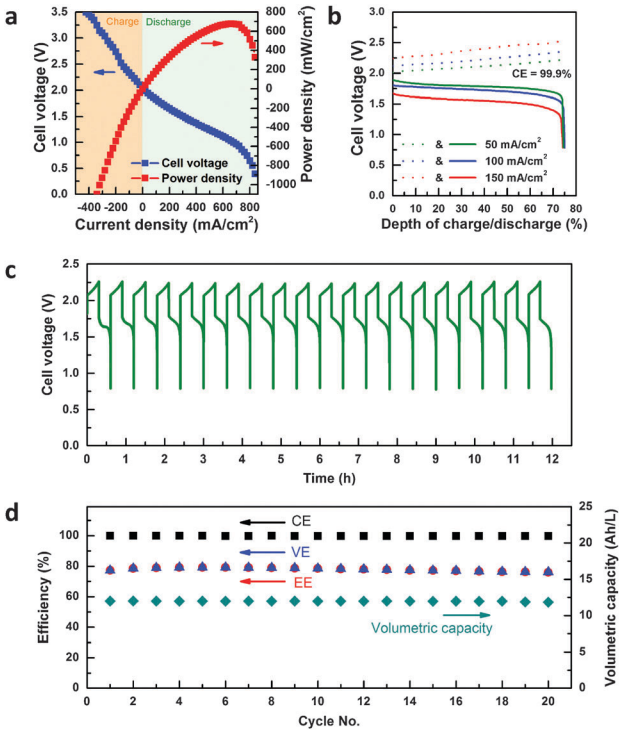

Fig. 3 Cell performance and the cycle test. (a) Charge and discharge polarization curve of the Zn–Fe RFB at 70% state of charge (SOC). Positive current density (in the light green region) represents the discharging process and negative current density (in light orange region) represents the charging process. (b) Charge–discharge test with a 75% SOC swing at 50, 100, and 150 mA cm^{-2} current density. The dash lines and solid lines represent the charging process and the discharging process, respectively. (c) Voltage curve of a 20-cycle test at 80 mA cm^{-2} with a 75% SOC swing. (d) Coulombic efficiency (CE), voltage efficiency (VE), energy efficiency (EE), and volumetric capacity of the experimental Zn–Fe RFB of each cycle.

isolation of two redox pairs, owing to the double-membrane cell configuration. In addition, the Zn–Fe RFB showed no decrease in coulombic efficiency (99.9%), voltage efficiency (76%) and capacity after 20 cycles at 80 mA cm^{-2} current density with 75% state of charge (SOC) swing (Fig. 3c and d).

Low element cost and high performance make the Zn–Fe RFB very attractive in terms of the total capital cost. To quantify the capital cost of the double-membrane RFB system, we adapted the cost model for all-V and Fe-V RFBs developed by

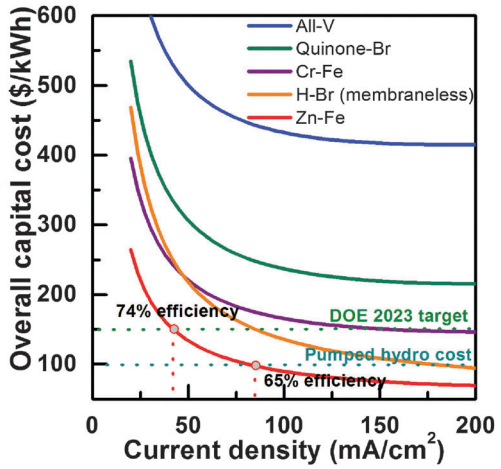

Fig. 4 Zn–Fe RFB cost analysis and comparison with other notable RFBs. Note that the long-term durability was not taken into account in the cost analysis in this work, and the cost comparison among different RFB technologies is only meaningful when they have the same or similar durability.

the Pacific Northwest National Lab (PNNL).[29] Based on the excellent PNNL model that (1) considered the geometry of cell, the configuration of stack, and auxiliary RFB components, (2) adopted the reliable pricing information, and (3) minimized the total capital cost, in this work we have expanded the model: (1) from a single-membrane configuration to a double-membrane configuration, and (2) from all-vanadium chemistry to various other redox chemistries. Note that the cost analysis was based on the small-scale experimental results. Although the model has already considered the performance losses during scaling up, the practical performance of the Zn–Fe RFB in a large scale may vary.

Fig. 4 shows the results of the total capital cost of a 1 MW/8 MW h system for Zn–Fe RFBs and a few most notable RFBs, including all-V,[29] quinone-bromide,[26] hydrogen-bromide (membraneless)[30] and chromium-iron.[18] Cost contributions and round-trip efficiency are also mapped over the range of current densities (Fig. S5, ESI†). At a current density of 40 mA cm^{-2}, a total capital cost of \$150 per kW h is projected (with 74% of overall energy efficiency at the system level), which meets the 2023 DOE's cost target (\$150 per kW h). Increasing current density will result in an even lower overall capital cost but decreased system efficiency, for example, a current density of 80 mA cm^{-2} (65% system efficiency) will lower the total capital cost to \$100 per kW h. It should be noted that the designed discharge duration is also an important factor determining the total capital cost of RFB systems. The system capital cost decreases with increasing discharge duration, and it is below \$150 per kW h when the discharge duration is greater than 5 hours (Fig. S6, ESI†). In this work, we focus on engineering the middle electrolyte, leaving out the optimization of membranes and electrodes common to most RFB efforts. The system efficiency is expected to be improved by further reducing the cell resistance *via* adopting highly-conductive and selective membranes and engineering electrodes.

Our results demonstrate that the Zn–Fe RFB can deliver high power density with inexpensive materials, making it the one of the most cost-effective RFB systems. The Zn–Fe RFB is able to meet the \$100 per kW h of the capital cost (with 65% system efficiency), although a significant amount of work is still needed such as long-term durability testing and scale-up to large cells and stacks before industrial implementation.

Acknowledgements

This work was funded by the US Department of Energy through ARPA-E Award (DE-AR0000346). We thank Vish Viswanathan of the PNNL for help and sharing details of the PNNL RFB's open-source cost model.

Notes and references

1 Z. G. Yang, J. L. Zhang, M. C. W. Kintner-Meyer, X. C. Lu, D. W. Choi, J. P. Lemmon and J. Liu, *Chem. Rev.*, 2011, **111**, 3577–3613.
2 J. Liu, J. G. Zhang, Z. G. Yang, J. P. Lemmon, C. Imhoff, G. L. Graff, L. Y. Li, J. Z. Hu, C. M. Wang, J. Xiao, G. Xia, V. V. Viswanathan, S. Baskaran, V. Sprenkle, X. L. Li, Y. Y. Shao and B. Schwenzer, *Adv. Funct. Mater.*, 2013, **23**, 929–946.
3 J. Rugolo and M. J. Aziz, *Energy Environ. Sci.*, 2012, **5**, 7151–7160.
4 U. Eberle, B. Muller and R. von Helmolt, *Energy Environ. Sci.*, 2012, **5**, 8780–8798.
5 H. Ibrahim, A. Ilinca and J. Perron, *Renewable Sustainable Energy Rev.*, 2008, **12**, 1221–1250.
6 U. Eberle, M. Felderhoff and F. Schuth, *Angew. Chem., Int. Ed.*, 2009, **48**, 6608–6630.
7 B. Dunn, H. Kamath and J. M. Tarascon, *Science*, 2011, **334**, 928–935.
8 P. Leung, X. H. Li, C. P. de Leon, L. Berlouis, C. T. J. Low and F. C. Walsh, *RSC Adv.*, 2012, **2**, 10125–10156.
9 W. Wang, Q. T. Luo, B. Li, X. L. Wei, L. Y. Li and Z. G. Yang, *Adv. Funct. Mater.*, 2013, **23**, 970–986.
10 M. Skyllas-Kazacos, M. H. Chakrabarti, S. A. Hajimolana, F. S. Mjalli and M. Saleem, *J. Electrochem. Soc.*, 2011, **158**, R55–R79.
11 A. Z. Weber, M. M. Mench, J. P. Meyers, P. N. Ross, J. T. Gostick and Q. H. Liu, *J. Appl. Electrochem.*, 2011, **41**, 1137–1164.
12 C. P. de Leon, A. Frias-Ferrer, J. Gonzalez-Garcia, D. A. Szanto and F. C. Walsh, *J. Power Sources*, 2006, **160**, 716–732.
13 Grid Energy Storage, U.S. Department of Energy, 2013.
14 R. F. Service, *Science*, 2014, **344**, 352–354.
15 D. S. Aaron, Q. Liu, Z. Tang, G. M. Grim, A. B. Papandrew, A. Turhan, T. A. Zawodzinski and M. M. Mench, *J. Power Sources*, 2012, **206**, 450–453.
16 N. H. Hagedorn, *NASA redox storage system development project final report*, National Aeronautics and Space Administration, Lewis Research Center, 1984.

17 J. Cheng, L. Zhang, Y. S. Yang, Y. H. Wen, G. P. Cao and X. D. Wang, *Electrochem. Commun.*, 2007, **9**, 2639–2642.
18 L. H. Thaller, 9th Intersociety Energy Conversion Engineering Conference Proceedings, 1974, 924–928.
19 L. Zhang, J. Cheng, Y. S. Yang, Y. H. Wen, X. D. Wang and G. P. Cao, *J. Power Sources*, 2008, **179**, 381–387.
20 M. C. Tucker, K. T. Cho and A. Z. Weber, *J. Power Sources*, 2014, **245**, 691–697.
21 S. Gu, K. Gong, E. Z. Yan and Y. S. Yan, *Energy Environ. Sci.*, 2014, **7**, 2986–2998.
22 R. Holze, *Landolt-Börnstein: Numerical Data and Functional Relationships in Science and Technology, Electrochemical Thermodynamics and Kinetics*, Springer, 2007.
23 R. D. Patel, K.-C. Lang and I. F. Miller, *Ind. Eng. Chem. Fundam.*, 1977, **16**, 340–348.
24 Y. Tanaka, *J. Membr. Sci.*, 2003, **216**, 149–164.
25 L. Zhang, H. Zhang, Q. Lai, X. Li and Y. Cheng, *J. Power Sources*, 2013, **227**, 41–47.
26 B. Huskinson, M. P. Marshak, C. Suh, S. Er, M. R. Gerhardt, C. J. Galvin, X. Chen, A. Aspuru-Guzik, R. G. Gordon and M. J. Aziz, *Nature*, 2014, **505**, 195–198.
27 M. L. Perry, R. M. Darling and R. Zaffou, *Stationary and Large Scale Electrical Energy Storage 2*, 2013, **53**, 7–16.
28 K. T. Cho, P. Albertus, V. Battaglia, A. Kojic, V. Srinivasan and A. Z. Weber, *Energy Sci. Technol.*, 2013, **1**, 596–608.
29 V. Viswanathan, A. Crawford, D. Stephenson, S. Kim, W. Wang, B. Li, G. Coffey, E. Thomsen, G. Graff, P. Balducci, M. Kintner-Meyer and V. Sprenkle, *J. Power Sources*, 2014, **247**, 1040–1051.
30 W. A. Braff, M. Z. Bazant and C. R. Buie, *Nat. Commun.*, 2013, 4.